High-Resolution Secondary Ion Mass Spectrometry Reveals the Contrasting Subcellular Distribution of Arsenic and Silicon in Rice Roots[1][C][W][OA]

Katie L. Moore*, Markus Schröder, Zhongchang Wu, Barry G.H. Martin, Chris R. Hawes, Steve P. McGrath, Malcolm J. Hawkesford, Jian Feng Ma, Fang-Jie Zhao, and Chris R.M. Grovenor

Department of Materials, University of Oxford, Oxford OX1 3PH, United Kingdom (K.L.M., M.S., C.R.M.G.); Rothamsted Research, Harpenden, Hertfordshire AL5 2JQ, United Kingdom (Z.W., S.P.M., M.J.H., F.-J.Z.); School of Life Sciences, Oxford Brookes University, Headington, Oxford OX3 0BP, United Kingdom (B.G.H.M., C.R.H.); and Institute of Plant Science and Resources, Okayama University, Kurashiki 710–0046, Japan (J.F.M.)

Rice (*Oryza sativa*) takes up arsenite mainly through the silicic acid transport pathway. Understanding the uptake and sequestration of arsenic (As) into the rice plant is important for developing strategies to reduce As concentration in rice grain. In this study, the cellular and subcellular distributions of As and silicon (Si) in rice roots were investigated using high-pressure freezing, high-resolution secondary ion mass spectrometry, and transmission electron microscopy. Rice plants, both the *lsi2* mutant lacking the Si/arsenite efflux transporter Lsi2 and its wild-type cultivar, with or without an iron plaque, were treated with arsenate or arsenite. The formation of iron plaque on the root surface resulted in strong accumulation of As and phosphorous on the epidermis. The *lsi2* mutant showed stronger As accumulation in the endodermal vacuoles, where the Lsi2 transporter is located in the plasma membranes, than the wild-type line. As also accumulated in the vacuoles of some xylem parenchyma cells and in some pericycle cells, particularly in the wild-type mature root zone. Vacuolar accumulation of As is associated with sulfur, suggesting that As may be stored as arsenite-phytochelatin complexes. Si was localized in the cell walls of the endodermal cells with little apparent effect of the Lsi2 mutation on its distribution. This study reveals the vacuolar sequestration of As in rice roots and contrasting patterns of As and Si subcellular localization, despite both being transported across the plasma membranes by the same transporters.

Arsenic (As) is a toxic element, and there may be no safe threshold below which it is not carcinogenic (Smith et al., 2002). The installation of tube wells in South and Southeast Asia to provide disease-free drinking water has resulted in what has been described as "the largest mass poisoning of a population in history" (Smith et al., 2000), with over 100 million people in Asia now exposed to As-contaminated drinking water (Brammer and Ravenscroft, 2009). Large areas of Bangladesh and West Bengal, India, are particularly badly affected because rice (*Oryza sativa*) is the staple crop in these countries, making up 73% of the calorific intake in Bangladesh (Meharg and Rahman, 2003). As-contaminated groundwater is used to irrigate rice paddies during the dry season, adding more than 1,000 tons of As to the soil each year in Bangladesh alone (Ali et al., 2003). Rice is inherently efficient in the uptake of As (Williams et al., 2007b; Su et al., 2010), which is further elevated when paddy fields are irrigated with As-contaminated water (Meharg and Rahman, 2003; Williams et al., 2006). Recent studies have shown that rice is a major source of inorganic As in diets where rice is the staple food (Ohno et al., 2007; Williams et al., 2007a; Mondal and Polya, 2008).

Arsenate is taken up by plant roots via phosphate transporters (Zhao et al., 2009); however, in submerged paddy field conditions, arsenite is the dominant form of As in the soil solution (Bogdan and Schenk, 2008; Xu et al., 2008). Arsenite, predominantly present at pH < 8 as $As(OH)_3$ due to its high pK_a (9.2), enters rice root cells through Lsi1, a Nodulin26-like intrinsic protein (NIP) aquaporin (NIP2;1; Ma et al., 2008). Lsi1 is a major influx transporter for silicic acid (Ma et al., 2006) and is also permeable to a range of

[1] This work was supported by the United Kingdom Engineering and Physical Sciences Research Council (grant no. GR/T19797), by the Biotechnology and Biological Sciences Research Council (grant no. BB/H006303/1), and by Grants-in-Aid for Scientific Research from the Ministry of Education, Culture, Sports, Science, and Technology of Japan (grant nos. 21248009 and 22119002 to J.F.M.).

* Corresponding author; e-mail katie.moore@materials.ox.ac.uk.

The author responsible for distribution of materials integral to the findings presented in this article in accordance with the policy described in the Instructions for Authors (www.plantphysiol.org) is: Katie L. Moore (katie.moore@materials.ox.ac.uk).

[C] Some figures in this article are displayed in color online but in black and white in the print edition.

[W] The online version of this article contains Web-only data.

[OA] Open Access articles can be viewed online without a subscription.

www.plantphysiol.org/cgi/doi/10.1104/pp.111.173088

small neutral (undissociated) molecules, including arsenite and methylated As species (Ma et al., 2008; Li et al., 2009a; Zhao et al., 2010c). Lsi1 is localized in the exodermis and endodermis, where the Casparian strips are formed, and this transporter is found on the distal side of the cells (Ma et al., 2006). A second silicon (Si) transporter, Lsi2, localized in the plasma membrane on the proximal side of same cells as Lsi1, mediates the efflux of Si (possibly silicic acid) from exodermal and endodermal cells toward the stele (Ma et al., 2007). Lsi2 is also able to transport arsenite; mutation of the *Lsi2* gene was found to result in a marked decrease in the concentration of arsenite in the xylem sap of rice, the accumulation of As in shoots, and the concentration in grain compared with the wild-type cultivars (Ma et al., 2008). Lsi2 appears to play a more important role in controlling As accumulation in the aboveground tissues than Lsi1. Increasing the silicic acid concentration in the soil solution was found to decrease As accumulation in rice shoots and grain (Bogdan and Schenk, 2008; Li et al., 2009b), probably through a competitive inhibition effect on arsenite transport via Lsi2 (Zhao et al., 2010b). Rice has a high requirement for Si as it plays important roles in defense against biotic and abiotic stresses (Ma and Yamaji, 2006). The efficient pathway for silicic acid uptake in rice inadvertently allows the accumulation of arsenite, which is mobilized under the anaerobic conditions of submerged paddy soils (Zhao et al., 2010b).

Despite silicic acid and arsenite sharing the same uptake pathway in rice roots, the translocation of silicic acid from roots to shoots is much more efficient than that of As; a typical concentration ratio of Si in the xylem sap to that in the external medium is around 20 (Mitani and Ma, 2005), whereas for As this is only 0.3 to 0.5 (Zhao et al., 2009). The reasons for this difference are not entirely clear, but it may be attributed to the propensity for arsenite to be extruded to the external medium (Xu et al., 2007; Su et al., 2010) or being complexed by thiol-rich peptides such as phytochelatins (Raab et al., 2005; Liu et al., 2010). Arsenite-thiol complexes are believed to be sequestered in the vacuoles of root cells, thus further decreasing the mobility of As toward the xylem, although direct evidence for the subcellular localization of As has not been presented for any nonhyperaccumulating plant species. There are a few studies on the Si distribution in the root cells of rice (Parry and Soni, 1972; Lux et al., 1999; Gong et al., 2006), showing that Si preferentially accumulates in the cell walls.

Rice is an aquatic plant that releases oxygen into the rhizosphere, oxidizing ferrous iron to ferric iron, which is then precipitated as iron (Fe) oxide/hydroxides onto the root surface, forming an Fe plaque (Armstrong, 1967). The presence of this Fe plaque may act as a barrier to the uptake of some potentially harmful metals or metalloids (Hansel et al., 2002; Liu et al., 2004). Both arsenate and arsenite are adsorbed onto Fe oxide/hydroxides, but the affinity is significantly less for arsenite (Liu et al., 2004; Fendorf et al., 2008). A study using excised roots showed that Fe plaque decreased arsenate uptake but increased arsenite uptake by rice (Chen et al., 2005). Although it is apparent that Fe plaque serves as a strong sink for As, its impact on As accumulation in rice is not clear.

Localizing the cellular and subcellular As distribution in plants with relatively low As concentrations is technically challenging, because most analytical instruments do not have the necessary combination of sensitivity and resolution, and the sample preparation needed to preserve the cellular and subcellular structures can be very challenging. Secondary ion mass spectrometry (SIMS) offers many advantages to the analysis of biological materials, in particular for the analysis of trace elements. The combination of high sensitivity, good lateral resolution, the ability to detect all elements and isotopes, molecular imaging, and three-dimensional analysis is unrivaled by any other technique (Burns, 1982; Chandra et al., 2000; Guerquin-Kern et al., 2005). NanoSIMS has been specifically designed for simultaneous high lateral resolution, high sensitivity, and high mass resolution analysis, meaning that the compromises between these characteristics are not as severe as they are for other analytical techniques including most SIMS instruments (Slodzian et al., 1992). Recent examples of biological studies by nanoSIMS include high-resolution imaging of the nickel distribution in a nickel hyperaccumulator plant (Smart et al., 2010), localization of As and Se in cereal grains (Moore et al., 2010), lipid distributions in phase-separated membranes (Kraft et al., 2006), and in situ mapping of nitrogen uptake in the rhizosphere (Clode et al., 2009). The SIMS technique has also recently been used to map, at subcellular resolution, Si and germanium in root and leaf tissues of annual blue grass (*Poa annua*) and orchard grass (*Dactylis glomerata*; Sparks et al., 2010).

SIMS analysis needs to be undertaken under high-vacuum conditions, which makes analysis of biological materials difficult due to their high water content (approximately 80%; Cooke and Kuntz, 1974; Mentré, 1992). While it has been shown that it is possible to analyze frozen hydrated samples with SIMS (Metzner et al., 2008, 2010a, 2010b), these experiments require very specialized equipment, give rise to complex elemental signals that require careful deconvolution, and the current resolution obtainable with this technique is limited to about 1 μm. Therefore, for most experiments, the water must be removed before SIMS analysis can be undertaken. However, preparing the sample to maintain not only the in vivo morphology of the sample but also the chemical distribution can be challenging. Ultrarapid cryofixation, for example high-pressure freezing (HPF), is now generally accepted to be the best method to preserve challenging materials and gives the best lateral resolution when cryoSIMS is not available (Steinbrecht and Zierold, 1987; Chandra et al., 2000).

Here, we show how high-resolution SIMS analysis in combination with HPF and transmission electron

microscopy (TEM) can be used to investigate the subcellular distribution of As and Si in rice roots and how they are influenced by the formation of the Fe plaque and by loss of function of Lsi2.

RESULTS

The Formation of Fe Plaque Results in Strong As Accumulation on the Epidermis

Rice roots were coated with an orange-colored Fe plaque after being treated with a ferrous sulfate solution for 24 h. Imaging the outer cell layers of the roots revealed the distribution of this Fe plaque. The black-and-white ion-induced secondary electron image shown in Figure 1 shows the four outer cell layers of the root: the epidermis in the bottom right, the exodermis, the sclerenchyma layer, and one layer of cells from the cortex in the top left. This image is typical of all the roots that were exposed to the ferrous solution, irrespective of whether the sample was treated with As(V) or As(III), and there was no difference, as expected, between the wild type and the *lsi2* mutant. The $^{12}C^{14}N^-$ image reveals some damage caused by the HPF. There are occasional breaks in the cell walls and membranes along either side of the sclerenchyma layer, but this does not prevent imaging of the Fe plaque, as the root is well preserved along the epidermis. The coaxial optics of the nanoSIMS means that the detected ions must have opposite polarity to the primary ion beam. The highest lateral resolution can be obtained using the Cs^+ beam, meaning that the Fe plaque was detected as the $^{56}Fe^{16}O^-$ ion. Complementary analysis was undertaken with an O^- beam to map $^{56}Fe^+$ (data not shown), and the same distribution was observed with both polarities, so we conclude that mapping the Fe plaque as $^{56}Fe^{16}O^-$ has not influenced the observed distribution. The $^{56}Fe^{16}O^-$ was only located on the epidermis of the root, indicating that the formation of Fe plaque occurs exclusively outside the exodermal cells, probably due to the blockage by the Casparian strip. The $^{56}Fe^{16}O^-$ distribution was not homogeneous along the epidermis; there were distinct regions of accumulation along the outer edge of the epidermis and along the boundary of the exodermis where entry is blocked. With the exception of $^{12}C^{14}N^-$, all the other imaged elements, $^{28}Si^-$, $^{31}P^-$, $^{32}S^-$ (data not shown), and $^{75}As^-$ [in both the As(V) and As(III) treatments], showed similar accumulation on the Fe plaque. The two Si hotspots associated with the sclerenchyma cells probably result from surface contamination rather than actual distribution of Si within the root. Where stronger $^{56}Fe^{16}O^-$ accumulation was observed, there was a similar stronger accumulation of As.

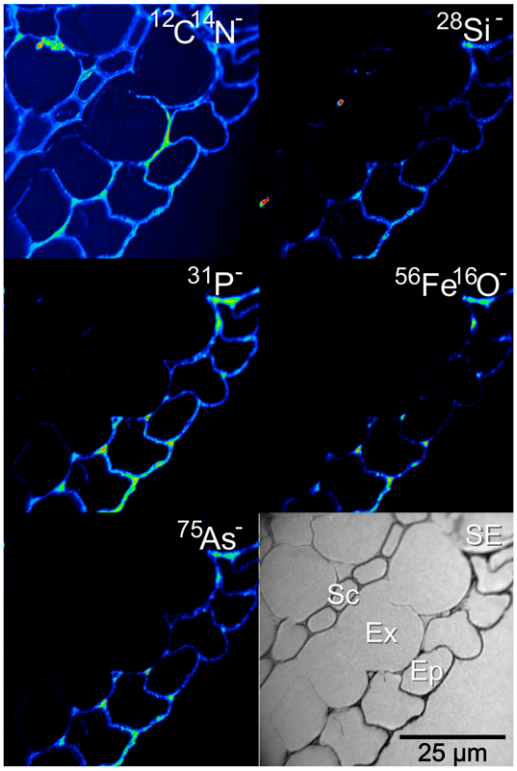

Figure 1. NanoSIMS image of the outer edge of an *lsi2* mutant near the root tip with Fe plaque and treated with silicic acid and arsenate, showing the outer four cell layers of the root with strong epidermal As colocalization with the Fe plaque (represented by the $^{56}Fe^{16}O^-$ image). Ep, Epidermis; Ex, exodermis; Sc, sclerenchyma; SE, secondary electron image. [See online article for color version of this figure.]

In contrast, roots that were not exposed to the ferrous solution did not show characteristic accumulation of Fe and As on the epidermis of the root. Very little As was detected on the outer surface of the roots, as shown in Supplemental Figure S1, and there was also no enhanced accumulation of Si, phosphorus (P), or sulfur (S) on the outer epidermis in comparison with the exodermal and sclerenchyma cells.

The Lsi2 Mutation Has No Effect on the Si or As Distribution in the Exodermis

The exodermis contains one of the two Casparian strips present in rice roots, with the Lsi2 transporter located on the proximal side of the exodermis. The Lsi2 transporter mediates the efflux of silicic acid and arsenite into the apoplast of the cortex cells, which degenerate to form aerenchyma in the mature zone of roots (Ma et al., 2007, 2008). As this transporter is nonfunctional in the mutant, accumulation of As and Si in the exodermis may have been expected; however, this was not observed. In all the mutant samples, there was neither detectable As accumulation in the exodermis nor obvious enhancement of Si in these cells compared with the wild-type samples (data not shown). Both the wild-type samples (data not shown) and the *lsi2* mutant showed some Si accumulation along the sclerenchyma (Fig. 1; Supplemental Fig. S1).

The Lsi2 Mutation Causes Vacuolar Accumulation of As in the Endodermis, Contrasting with Cell Wall Accumulation of Si Unaffected by the Mutation

Imaging of the stele region of the *lsi2* mutant treated with ferrous sulfate solution, silicic acid, and As(V) revealed the distributions of As and Si at high resolution (Fig. 2). One of the major xylem vessels is situated in the top right corner of the image as shown in the secondary electron image, and the endodermis where the second Casparian strip is situated can be seen across the center of the image. The $^{12}C^{14}N^-$ image reveals many cellular details indicating the presence of the membranes, nuclei, and vacuoles. Conventional sample preparation procedures such as chemical fixation do not preserve the chemical distribution of diffusible species (Chandra et al., 2000), for example, ions in the vacuoles; however, it can be seen that a uniform As accumulation in the endodermal vacuoles has been preserved by HPF (Fig. 2).

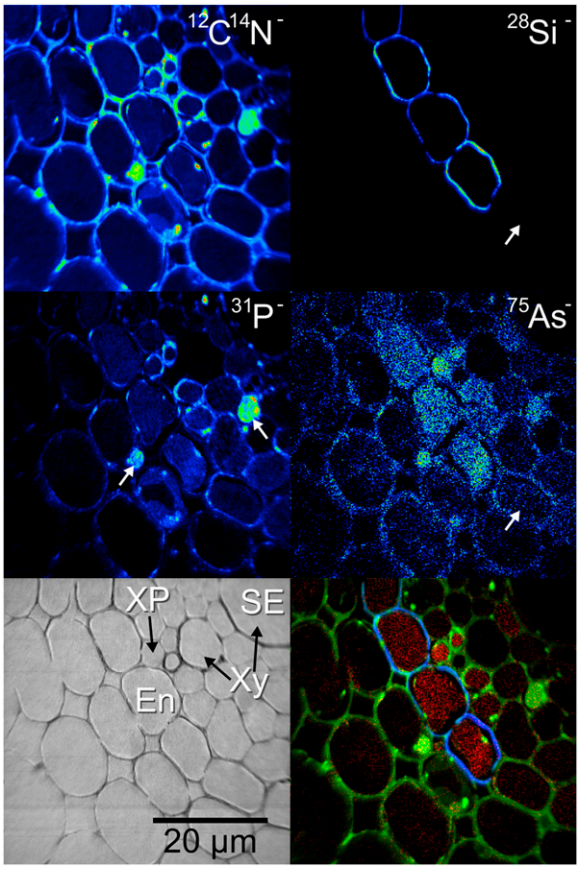

Figure 2. NanoSIMS image of the stele region of an *lsi2* mutant from near the root tip treated with arsenate, showing As accumulation in the vacuoles of the endodermis with Si localized around the same cells. The color merge image shows the relative locations of $^{75}As^-$ (red), $^{12}C^{14}N^-$ (green), and $^{28}Si^-$ (blue). The white arrows on the $^{31}P^-$ image indicate the positions of nuclei, and the white arrows on the $^{28}Si^-$ and $^{75}As^-$ images indicate cells with no Si or As accumulation. En, Endodermis; SE, secondary electron image; XP, xylem parenchyma; Xy, xylem. [See online article for color version of this figure.]

Si was found to be localized in characteristic rings in the endodermal cell walls (see below for evidence of its cell wall localization), with no obvious differences in intensity observed on the distal or proximal side (Fig. 2). The $^{12}C^{14}N^-$ image reveals several subcellular details. Vacuoles can be observed in the endodermis, several of which have separated from the cell walls along with some of the cytoplasm, a sign of damage during the HPF process. The white arrows in the $^{31}P^-$ image, along with the high intensities in the $^{12}C^{14}N^-$ image, reveal the presence of two nuclei located in cells on either side of the endodermis. The $^{75}As^-$ image reveals the accumulation of As in the vacuoles of the endodermis in root cells. This accumulation was possibly a result of the Lsi2 mutation, since such a strong localization was not observed in the endodermis of wild-type roots (Fig. 3). Imaging of the whole endodermis around the stele in a series of nanoSIMS images revealed a similar pattern of As accumulation in the vacuoles. Not all of the endodermal cells, however, were outlined with Si; there were several endodermal cells without strong Si signals, which in some cases coincided with no accumulation of As in the vacuole of that cell. This is shown by the white arrows in the $^{28}Si^-$ and $^{75}As^-$ images for the lower endodermal cell in Figure 2.

In contrast to the *lsi2* mutant, analysis of the wild-type samples did not show any strong As accumulation in the endodermis of the roots (Fig. 3), which is as expected because the Lsi2 transporter is able to efflux As into the stele for loading into the xylem. As was only localized to the cell walls and membranes with some accumulation in the metabolically active regions of the cells, for example, in the nucleus of the middle endodermal cell, as indicated by the white arrow. Surprisingly, there was no difference in the Si distribution between the wild type and the *lsi2* mutant. In both cases, the Si was localized in the endodermal cell walls, again with no obvious differences between the concentration at the proximal and distal sides.

As Accumulation in the Pericycle and Xylem Parenchyma

A markedly different distribution of As was observed in the *lsi2* mutant treated with silicic acid and arsenate. Instead of As accumulation in the endodermis, As accumulated in the pericycle, the layer of cells immediately inside the endodermis (Fig. 4). This also corresponded with a complete lack of Si detected in the endodermis. It is likely that this was from a younger portion of the root where the Casparian strip had not formed, and the Si transporters are less expressed in this region (Yamaji and Ma, 2007).

Imaging of the As distribution in a mature root zone (approximately 20 cm from the tip) of a wild-type root revealed that although there was some accumulation of As in the vacuoles of the endodermis, a very high As

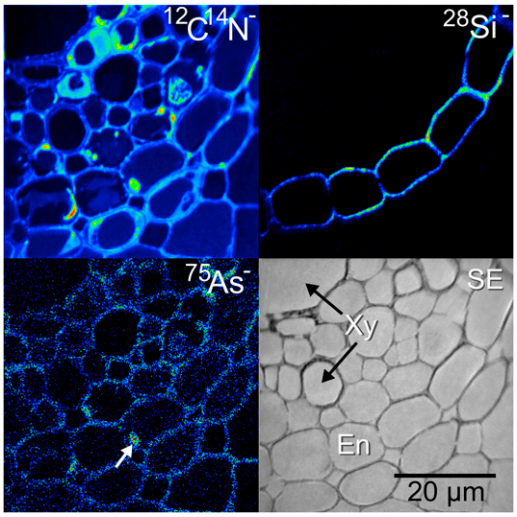

Figure 3. NanoSIMS image of the stele region from a wild-type root near the root tip treated with arsenate, showing no As accumulation in the vacuoles of the endodermis. Si is localized around the endodermal cells with the same distribution pattern as in the *lsi2* mutant (Fig. 2). En, Endodermis; SE, secondary electron image; Xy, xylem. [See online article for color version of this figure.]

intensity was detected in the pericycle cell vacuoles. The higher As signal in this sample was partly due to a longer period of As exposure (2 weeks). This strong As signal was colocalized with a very strong S signal (Fig. 5).

A recurring feature in all the roots, irrespective of the species of the As applied, is the significant As accumulation in some of the xylem parenchyma cells. This feature was more common in the *lsi2* mutant, although it was also observed in the wild-type roots both close to the tip and in the mature zone and is also more common in the treatments without a Fe plaque. The xylem parenchyma also contained a high concentration of S. Some examples of this are presented in Figure 6.

Si Is Localized to the Cell Walls of the Endodermis

As it was not clear from the nanoSIMS images in which part of the cell the endodermal Si was localized, complementary TEM analysis was undertaken on adjacent thin sections of the root, as TEM can provide cellular information at a higher resolution than the nanoSIMS. An ultrathin section was cut for TEM analysis, followed by a 1-μm section for the nanoSIMS analysis. The same sections were not used for both techniques, as the ultrathin TEM sections were not sufficiently mechanically stable for nanoSIMS analysis. The TEM indicated that the majority of the endodermal cell walls contained a thin line of dark features (indicated by white arrows in Fig. 7, B and C). The distribution was similar to that observed for Si in the nanoSIMS, with these features being entirely absent in some cell walls. To determine if these dark features were in fact rich in Si, neighboring cell walls were identified, one containing these features and the other without. The same cells were then located in the nanoSIMS section, and a high-resolution image was acquired. Figure 7A shows two endodermal cells: the left has dark features in the cell walls, and the right does not. This is shown more clearly in the higher resolution images (Fig. 7, B and C). These higher resolution images also show some of the damage caused by the HPF process. Breaks in the cell walls can be seen (Fig. 7, A and C), and the higher resolution images clearly show that the contents of the cell, including the cytoplasm in some cases, have pulled away from the cell walls. The nanoSIMS image (Fig. 7D) clearly shows that the dark features in the TEM images are in fact Si rich. Only the left cell contains Si (shown in blue), corresponding exactly with the dark features in the TEM images of Figure 7, B and C. The $^{12}C^{14}N^-$ image, represented in green, shows that there is high signal from the cell walls, membranes, and cytoplasm, with a lower signal originating from the vacuoles. At the top of the nanoSIMS image, the red arrow indicates the position and direction of a line scan taken across the cell wall (Fig. 7E). Both the image and the line scan show that the $^{12}C^{14}N^-$ signal from the cell wall falls mainly outside of the Si signal. The highest $^{12}C^{14}N^-$ signal originates from the cell wall and the lower peak comes from the vacuolar membrane, with the $^{28}Si^-$ peak consistently falling inside of the cell wall $^{12}C^{14}N^-$ peak across all the samples analyzed, both wild type and the *lsi2* mutant. From the TEM images, it is clear that the higher $^{12}C^{14}N^-$ signal

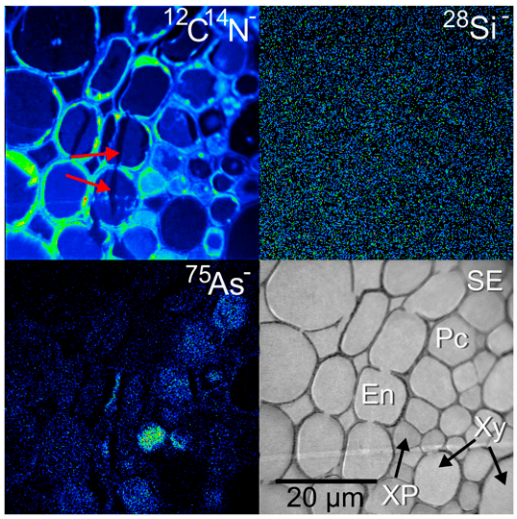

Figure 4. NanoSIMS image of the stele region of an *lsi2* mutant from near the root tip treated with silicic acid and arsenate, showing As accumulation in the vacuoles of the pericycle. No localization of Si was detected in this region. En, Endodermis; Pc, pericycle; SE, secondary electron image; XP, xylem parenchyma; Xy, xylem. The red arrows on the $^{12}C^{14}N^-$ image indicate where there has been HPF damage, resulting in a split across the cells subsequently filled with resin. [See online article for color version of this figure.]

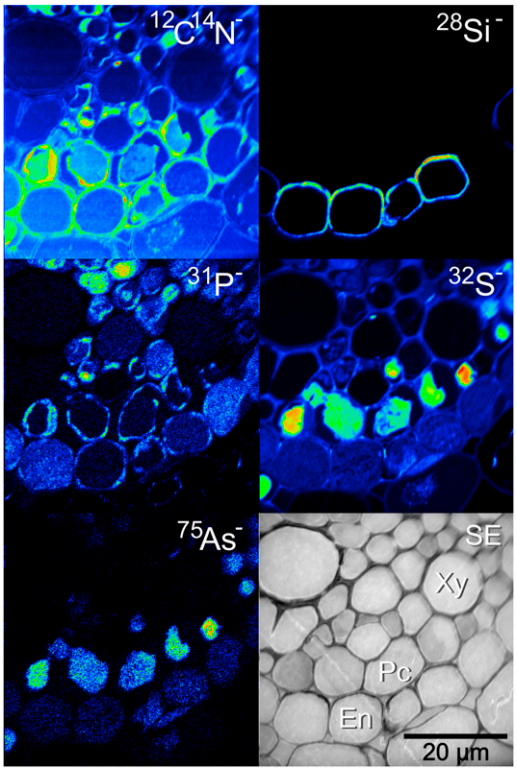

Figure 5. NanoSIMS image of the stele region of the mature zone of a wild-type root treated with silicic acid and arsenite, showing some As accumulation in the endodermis and very strong As accumulation in the vacuoles of the pericycle colocalized with a strong S signal. The proximal side of the endodermal cells is noticeably thicker, corresponding with a higher Si concentration. En, Endodermis; Pc, pericycle; SE, secondary electron image; Xy, xylem. [See online article for color version of this figure.]

relates to the darker cell wall material and that the lighter gray cell wall where the Si is localized yields very little $^{12}C^{14}N^-$ signal.

Imaging of the mature zone of wild-type roots, approximately 20 cm from the tip, showed an almost identical distribution of Si (i.e. Si is localized to the cell walls and completely surrounds the endodermis). The only differences in the distribution was that the dark features observed in the TEM extended throughout the entire cell wall, rather than a thin line toward the outside edge of the cell, and that the proximal side of the endodermal cell walls was distinctly thicker than the distal side. The TEM and nanoSIMS images from the same cell are shown in Supplemental Figure S2. NanoSIMS imaging revealed that the Si signal originated from a much thicker region of the cell wall and that the intensity was much higher on the proximal side, as also shown in Figure 5.

Quantitative Analysis of As Concentrations

Considerable care has to be taken to obtain quantitative data in SIMS analysis (Dérue et al., 2006b), because, for instance, the effect of surface topography and differences in the primary ion current prevented a direct comparison of the As counts from each of the analyzed areas. To quantify the nanoSIMS data from different samples, the total number of $^{75}As^-$ counts was normalized with the total number of counts in the corresponding $^{12}C^{14}N^-$ image. Normalization with $^{12}C^{14}N^-$ has been found to be a useful approach to avoid these potential sources of error and allow a direct comparison between different samples and treatments (Follet-Gueye et al., 1998; Dérue et al., 2006a). Normalization was repeated for all of the analyzed regions of interest, and where possible, the results were summed over several roots from the same treatments. For some treatments, the sample preservation was relatively poor, leading to fewer analyzable roots; hence, there are larger errors in these data sets. The total As concentration of whole roots was determined by inductively coupled plasma mass spectrometry (ICP-MS), and because the nanoSIMS only analyzes a few cells, in one image, the nanoSIMS data have been collated by adding values from the edge of the roots to the data from the center of the roots to get representative ratios from the whole section. The ratios from the nanoSIMS were then compared with the ICP-MS data, as shown in Figure 8. For a comparison between the two data sets, the nanoSIMS data for the wild-type sample treated with ferrous Fe and As(III) has been scaled to match that of the ICP-MS data for this treatment. The errors on the nanoSIMS data have been calculated by adding together the SD values for the edge and stele data. There is good relative agreement between the ICP-MS and nanoSIMS data, suggesting that the sample preparation for SIMS analysis has not removed As to any great extent.

DISCUSSION

The results from this study have shown that high-resolution SIMS analysis, in combination with ultrarapid HPF and TEM, are powerful tools in understanding the uptake and storage of As in rice roots by imaging the distribution with subcellular resolution. Previous work that has attempted to localize As in plant roots of *Phalaris arundinacea* (Hansel et al., 2002) and rice (Smith et al., 2009; Seyfferth et al., 2010) had indicated where the As was localized, but the resolution was too poor to precisely locate the elements to a particular cell layer or part of the cell.

The majority of our root samples were well preserved by HPF, allowing us to be confident that the sample preparation has not altered significantly the in vivo chemistry and also allows successful high-resolution imaging. As shown in Figures 4 and 7, in some cases, damage to the cells has been caused by the HPF process, in particular fracturing of the cell walls and the separation of the cytoplasm from the cell walls. Usually, this did not affect the distribution of the elements in the areas of interest. For instance, the

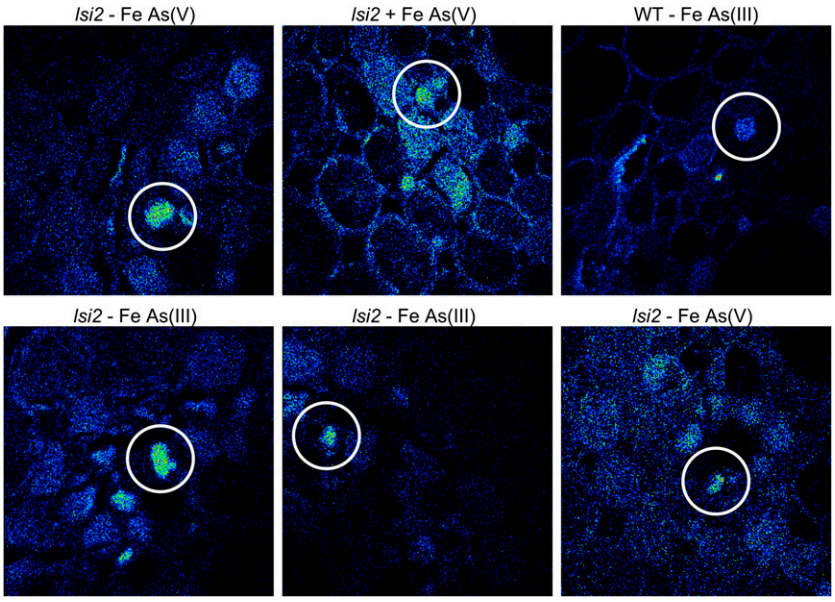

Figure 6. NanoSIMS images of $^{75}As^-$ showing As accumulation in xylem parenchyma cells near the root tip, as indicated by the white circles. This accumulation is more common in the *lsi2* mutants; however, it has also been observed in one wild-type cell (top right). Only the image in the top middle is from a sample treated with a ferrous solution. All images are 50 μm × 50 μm. [See online article for color version of this figure.]

uniform distribution of As in the vacuoles of the endodermal cells gives us confidence that the sample preparation has not significantly altered the As distribution, even though vacuolar As is likely to be highly diffusible and is therefore the most likely area where redistribution could have occurred. In addition, imaging of the highly diffusible cations, Na^+ and Ca^+ (Supplemental Fig. S3), indicated that the sample preparation method had not seriously redistributed these ions, which are difficult to preserve in their in vivo location. Different roots with the same treatment show very similar results, also suggesting that the sample preparation has not altered the elemental distributions.

Substantial care has to be taken to ensure that reliable composition data are achieved by SIMS analysis. It is well understood in the SIMS community, for instance, that it is very difficult to quantify SIMS data, mainly due to the well-known matrix effect (Wilson et al., 1989). Complex protocols are needed to perform robust quantitative SIMS analysis, ideally requiring the establishment of relative sensitivity factors specifically for the material in question (Dérue et al., 2006b). This becomes very difficult with biological materials because there tend to be large variations in density and composition between different components of the cell (e.g. the nucleus is structurally and chemically very different from the cell walls). However, this matrix effect is most severe when analyzing elements at concentrations greater than 1,000 $\mu g\ g^{-1}$, while at lower concentrations, a linear relationship between the measured and actual concentration still holds (Vickerman and Gilmore, 2009). For this study, therefore, with As concentrations in the few hundred $\mu g\ g^{-1}$ range, the effect of the different biological matrices on yield of As has been assumed to be negligible, and the local As signal detected can be assumed to be representative of the actual concentration differences in the sample. As shown in Figure 8, the nanoSIMS data show good agreement with the ICP-MS data for bulk As concentration variations. This suggests that the sample preparation has not significantly altered the As distribution or concentration and that our methodology can be used to quantify the nanoSIMS data.

The formation of Fe plaque is a common feature of rice roots growing in submerged soils. The effect of the Fe plaque was very distinct and obvious in both Figure 1 and in the quantitative data of Figure 8. The Fe plaque resulted in a high accumulation of the As on the epidermis, as would be expected with adsorption of As(V) or As(III) by the Fe oxyhydroxides (mainly ferrihydrite; Hansel et al., 2001). Stronger $^{56}Fe^{16}O^-$ accumulation was associated with stronger As accumulation, as would be expected considering the strong affinity of Fe plaque for As (Liu et al., 2004; Fendorf et al., 2008). This colocalization has also been shown in rice roots with x-ray tomography (Seyfferth et al., 2010). Line scans across the epidermal cells revealed that the Fe plaque was predominantly localized outside the plasma membranes of the epidermal cells, but some Fe was detected inside the cell plasma membrane (data not shown). The Fe plaque is composed of fine needles about 10 nm thick and 200 to 300 nm long, as shown by TEM (Supplemental Fig. S4), and this is why the Fe plaque does not appear as a sharp line in the nanoSIMS images. This distribution is similar to that observed previously (Green and Etherington, 1977) but is presented here at higher resolution. This TEM image also shows that some Fe plaque is present inside the cell, albeit at lower density, consistent with the nanoSIMS line scans. The reason for the Fe plaque penetrating the membrane of the epidermis is probably because these cells were dead.

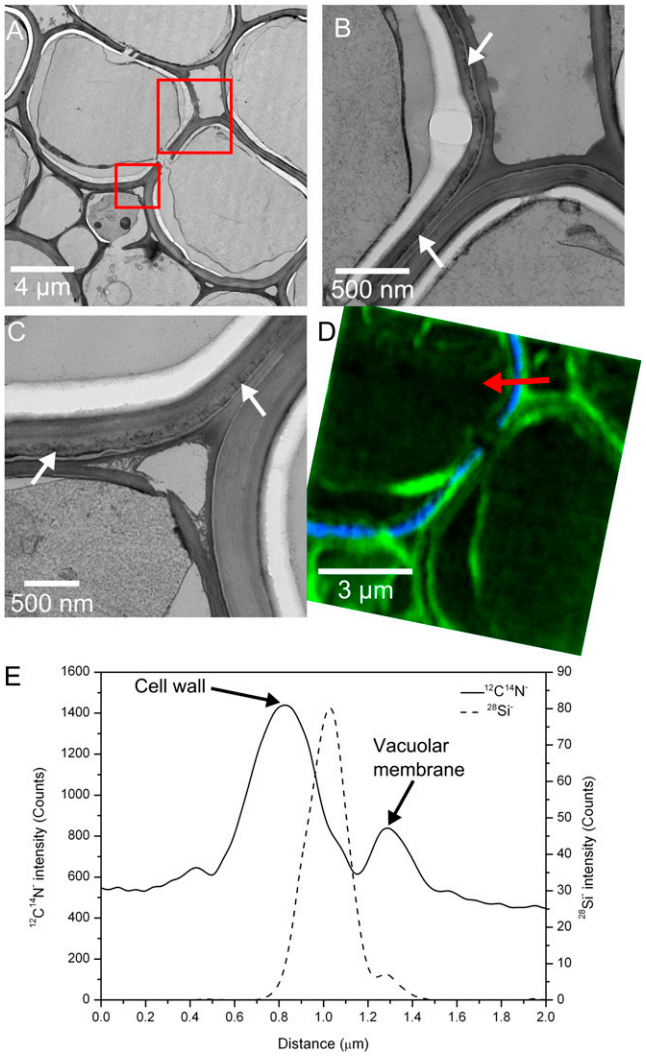

Figure 7. Combined TEM and nanoSIMS analysis indicating that Si is localized to some but not all endodermal cell walls. An overview of two endodermal cells is shown in A, with the red squares indicating the locations of the higher magnification TEM images shown in B and C. White arrows indicate the positions of the dark Si-rich features. The nanoSIMS image in D is taken from an adjacent section, and the relative positions of the $^{12}C^{14}N^-$ and $^{28}Si^-$ signals are shown in green and blue, respectively. The red arrow in D indicates the position of the line scan in E, showing that the $^{12}C^{14}N^-$ and $^{28}Si^-$ signals originate from different locations in the cell wall. [See online article for color version of this figure.]

There was no observable difference in the distribution of As adsorbed onto the Fe plaque between the samples treated with arsenite or arsenate. It is likely that oxygen released by the roots of the arsenite-treated samples into the rhizosphere resulted in some local oxidation of arsenite to arsenate, which was then adsorbed onto the root epidermis. Alternatively, adsorbed arsenite may be oxidized to arsenate on the Fe plaque. Other elemental signals, including $^{31}P^-$ and $^{28}Si^-$, show strong association with the Fe plaque. This study has presented detailed information on the morphology and localization of Fe plaque and the colocalization of As and other elements with the plaque, which can aid understanding of the mechanism of sequestration of As and other important elements at the root surface.

To our knowledge, this study is the first time that the accumulation of As in the vacuoles of root cells has been observed in a nonhyperaccumulator species. Previously, vacuolar accumulation of As has only been reported in the fronds of the As hyperaccumulator fern *Pteris vittata*, which contained As concentrations 1 to 2 orders of magnitude higher than those in the rice roots in our study (Lombi et al., 2002; Pickering et al., 2006). Vacuolar sequestration of As has been proposed as an important mechanism of As detoxification (Bleeker et al., 2006; Zhao et al., 2009). In As hyperaccumulating ferns, As is stored in the fronds mainly as uncomplexed arsenite (Lombi et al., 2002; Wang et al., 2002; Zhang et al., 2002; Pickering et al., 2006). Recently, an arsenite efflux transporter (PvACR3) localized to the tonoplast in As hyperaccumulators has been shown to mediate arsenite transport into the vacuoles and to play an important role in As detoxification (Indriolo et al., 2010). In contrast, As is stored mainly as arsenite-phytochelatin complexes in As nonhyperaccumulators (Raab et al., 2005; Liu et al., 2010), and these are likely the main forms of As observed in the vacuoles of rice roots. Indeed, in the cells showing strong As accumulation in the endodermal vacuoles, there were also elevated S signals (Supplemental Fig. S5), and this colocalization is very apparent in the vacuoles of the pericycle in the mature root zone (Fig. 5) and in the xylem parenchyma, suggesting that the majority of As in rice roots is stored as arsenite-phytochelatin complexes. Recently, two ABCC-type transporters have been identified in

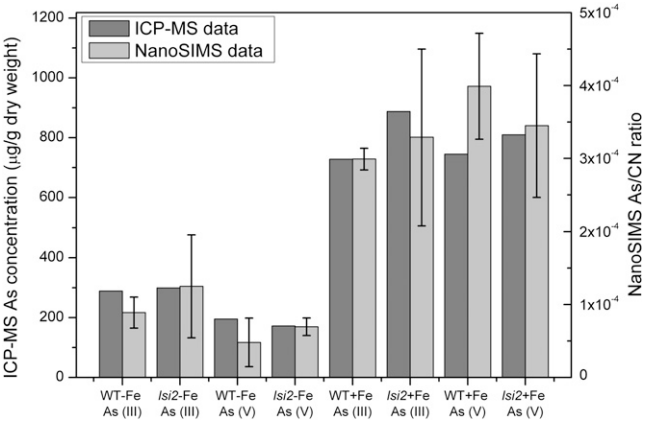

Figure 8. ICP-MS and nanoSIMS data for each treatment. ICP-MS data show the total concentration of As in the roots. The nanoSIMS data show the summed (edge and stele) $^{75}As^-/^{12}C^{14}N^-$ ratio and have been scaled to the wild-type (WT) + Fe As (III) ICP-MS data for comparison. Error bars on the nanoSIMS data represent the summed SD values from the edge and stele regions. ICP-MS analysis was performed on one replicate of the root samples.

Arabidopsis (*Arabidopsis thaliana*) as the major vacuolar transporters for arsenite-phytochelatin complexes (Song et al., 2010) that are required for As detoxification. In our study here, we did not observe a great difference in the As localization between the As(V) and As(III) treatments. This similarity can be explained by a rapid reduction of arsenate to arsenite in root cells. Xu et al. (2007) showed that more than 90% of the As taken up by rice roots from the arsenate treatment was reduced to arsenite within 1 d of As exposure.

Interestingly, these new nanoSIMS data show that the endodermis, pericycle (especially in the mature root zone), and xylem parenchyma cells are the main locations of As storage in rice roots (Figs. 2 and 4–6), while the outer cells in rice roots store little As. A concentration effect may be expected as a result of the radial transport of solutes from the outer cells to the stele. Alternatively, this pattern may reflect the sites where arsenite-thiol complexation and subsequent vacuolar transport are most active. Differences between the *lsi2* mutant and wild-type roots were observed, with the mutant showing a more pronounced accumulation of As in the vacuoles of the endodermal cells, whereas the wild-type roots showed accumulation in the pericycle cells. This difference can be attributed to the disruption in the mutant of the Lsi2 transporter, which is localized to the proximal sides of the exodermis and endodermis (Ma et al., 2007); hence, As cannot be effluxed into the stele. It is not clear why the mutant did not accumulate more As in the exodermis than in the endodermis, but the lack of strong exodermal accumulation of Si and As in *lsi2* may be caused by efflux of these elements to the epidermal apoplast and the external medium via Lsi1, a passive transporter allowing bidirectional flux of silicic acid and As(III) (Mitani et al., 2008; Zhao et al., 2010a). For the root shown in Figure 4, where As accumulation was observed in the pericycle of the *lsi2* young root zone, knocking out the Lsi2 transporter may have little effect, because in this section of root the Casparian strip may not be fully developed, allowing solutes to pass freely through the endodermis into the stele. This would allow the accumulation of As inside the stele and would explain the lack of Si accumulation, as the transporters are less expressed in this region. A strong As accumulation in the pericycle cells is observed in the mature root zone from a wild-type plant along with some endodermal accumulation in the vacuoles, as well as a preferential accumulation of Si on the proximal side of the endodermal cell walls (Fig. 5; Supplemental Fig. S2). These patterns could be attributed, at least in part, to the function of Lsi2. Accumulation of As in the pericycle in the wild-type plants may explain why little difference was observed in the root As concentration between the wild-type and *lsi2* mutant samples (Fig. 8; Ma et al., 2008); when Lsi2 is functional, As accumulates in the pericycle, and when this transporter is knocked out, As accumulates in the endodermal vacuoles.

In addition to As accumulation in the endodermis, another recurring feature, irrespective of whether the sample was treated with As(III) or As(V) and also in the mature root zone, was the accumulation of As in the xylem parenchyma. The function of these cells is to transport ions into the xylem vessels (Läuchli et al., 1974), and the fact that the As is accumulated here before being transported into the xylem may indicate a key transport pathway into the plant. This observation was more apparent in the *lsi2* mutant samples and the treatments without Fe plaque, which is also consistent with increased As concentration in the shoots with no-Fe plaque treatments (Fig. 6).

Strong accumulation of Si was also found in the endodermis of both the wild type and the *lsi2* mutant. However, in contrast to the vacuolar accumulation of As, Si was found to be localized to the cell walls (Figs. 2 and 3). The difference between As and Si may be because of the absence of transporters to transport Si into the vacuole for storage, and this would also explain, at least partly, the much higher root-to-shoot translocation of Si than As in rice. The lack of a difference between *lsi2* and the wild type was unexpected, but perhaps not surprising, considering that the two lines of rice differ significantly only in the shoot Si concentration and not in the root Si concentration (Ma et al., 2007).

A few previous studies, using techniques with a lower lateral resolution than the results presented here, have shown Si localization in the endodermis of rice roots (Parry and Soni, 1972; Lux et al., 1999; Gong et al., 2006). However, in these studies, with the exception of Parry and Soni (1972), Si appears to localize only to the proximal side of the endodermis rather than completely surrounding the cell, as observed in our studies. Similarly, Sparks et al. (2010) mapped the Si distribution in the roots of two grass species (*P. annua* and *D. glomerata*) and found the same distribution, with the Si localized only to the proximal side of the endodermis. Gong et al. (2006) stated that in their study, the Si was found to be a component of the root cell walls, and Parry and Soni (1972) concluded that more Si was localized on the inner tangential walls, which is consistent with our observations. A possible explanation for the discrepancy between this study and others could be related to the concentration and duration of the Si supply to the plants. In the previously published studies, the duration of the Si supply was longer or the concentration was higher than the relatively low concentration of 1 mM used in this study. For the wild-type samples, Si can be transported across the endodermis by Lsi1 and Lsi2, and if the Si concentration is very high, strong proximal accumulation of Si in the endodermal cell walls could be caused if Si efflux from the endodermis is greater than Si loading into the xylem, as observed in the mature root zone (Fig. 5) and the previous studies of Parry and Soni (1972), Lux et al. (1999), Gong et al. (2006), and Sparks et al. (2010). For the *lsi2* mutant roots in this study, an accumulation on the distal side

of the endodermis may not be observed due to the low concentration and short duration of Si supplied. It is also possible in the x-ray microanalysis studies of Gong et al. (2006) and Lux et al. (1999) that there was insufficient resolution and/or sensitivity to detect the lower concentration on the distal side, clearly revealed by the nanoSIMS, and hence the results could be similar.

In conclusion, this study has shown the potential of using high-resolution secondary ion mass spectrometry in combination with TEM to localize As in the roots of rice plants, revealing a contrasting subcellular distribution of As and Si in the roots. Where the Fe plaque forms on the root epidermis (e.g. under anaerobic conditions), it serves as a strong sink for both As(V) and As(III). Inside rice roots, As is stored in the vacuoles of the endodermis, pericycle, and xylem parenchyma cells. Colocalization of S with As in these vacuoles supports the notion that As is stored as arsenite-phytochelatin complexes. Mutation of the Lsi2 transporter results in stronger vacuolar accumulation of As in the endodermal cells compared with the wild type, where pericycle accumulation is observed. Si is localized to the cell walls of the endodermis both near the tip and in the mature roots, and this distribution is apparently not strongly affected by the Lsi2 mutation.

MATERIALS AND METHODS

Plant Materials and Culture

Two lines of rice (*Oryza sativa*), the *lsi2* mutant (Ma et al., 2007) and its wild-type cv T-65, were used. Seeds were surface sterilized with 0.5% NaOCl for 15 min, rinsed thoroughly with deionized water, and placed on a nylon net floating on a 0.5 mM $CaCl_2$ solution. After germination, seedlings were transferred to 0.35-L pots (four plants per pot) filled with half-strength Kimura solution and precultured for 3 weeks. The nutrient composition was as follows: 0.091 mM KNO_3, 0.183 mM $Ca(NO_3)_2$, 0.274 mM $MgSO_4$, 0.1 mM KH_2PO_4, 0.183 mM $(NH_4)_2SO_4$, 0.5 μM $MnCl_2$, 3 μM H_3BO_3, 0.1 μM $(NH_4)_6Mo_7O_{24}$, 0.4 μM $ZnSO_4$, 0.2 μM $CuSO_4$, 40 μM NaFe(III)-EDTA, and 2 mM MES (pH adjusted to 5.5 with KOH). Nutrient solution was renewed every 3 d. The growth conditions were a 16-h photoperiod with a light intensity of 500 μmol m^{-2} s^{-1}, 30°C/25°C day/night temperatures, and 70% relative humidity. To induce Fe plaque formation, rice seedlings were placed in deionized water overnight and then in 2 mM $FeSO_4$ (pH adjusted to 5.5 with KOH) for 24 h (Liu et al., 2004). Plants were transferred into deionized water for 6 h to remove extra ferrous ions from the root surface. Another group of plants not treated with $FeSO_4$ was used as the control. All seedlings were transferred to a nutrient solution with 1 mM silicic acid for 2 d before the As treatments were started. Both arsenate and arsenite were supplied at a concentration of 10 μM, and the As exposure lasted for 3 d. Three of the treated seedlings were used for nanoSIMS analysis. One of the treated seedlings was analyzed for total As concentration in the roots and shoots by ICP-MS (Agilent ICP-MS 7500ce; Agilent Technologies) following acid (HNO_3:$HClO_4$, 85:15) digestion.

In an additional experiment, wild-type rice plants were grown in the half-strength Kimura nutrient solution up to the flag leaf stage (one plant per 1-L pot). Plants were then exposed to 1 mM silicic acid and 10 μM arsenite for 2 weeks before the root samples were prepared for nanoSIMS analysis.

Sample Preparation for NanoSIMS Analysis

Rice roots were sectioned under MES buffer. Segments of the root, 2 to 2.5 mm in length, were taken at 2 cm from the tip of the root using a scalpel blade, taking care not to squash the root. Mature roots were cut at approximately 20 cm from the root tip from plants that were grown in the additional experiment. These root segments, approximately 0.4 to 0.5 mm in diameter, were then placed into 3-mm-diameter planchettes and coated with hexadecene, a nonpenetrating cryoprotectant. Another planchette was placed on top and immediately frozen in a Bal-Tec HPM 010 high-pressure freezer, freezing the sample at a pressure of 210 MPa at −196°C for a duration of 30 ms. Immediately after freezing, the planchettes were split apart and stored under liquid nitrogen before being transferred into microporous pots under liquid nitrogen, covered with acetone slush, and capped. Freeze substitution was carried out using a Reichert AFS (Leica) freeze-substitution system that was precooled to −160°C. Individual microporous pots were placed on top of acetone slush in universal aluminum containers into the freeze-substitution system along with an equal number of aluminum containers containing 2% osmium tetroxide in acetone (HPLC grade). The freeze-substitution apparatus was programmed to maintain −160°C for 30 min before heating the sample at a rate of 15°C h^{-1} to −85°C, where the temperature was maintained for 24 h, at which point the acetone melts and the specimen microporous pots were transferred into the thawed osmium solution. The freeze-substitution machine was then programmed to −85°C for 26 h, heating at a rate of 2°C h^{-1}, 8 h at −60°C, heating at a rate of 2°C h^{-1}, 24 h at −30°C, heating at a rate of 1°C h^{-1}, and finally held at −20°C for 24 h. At this point, samples were removed from the freeze-substitution system and transferred to a refrigerator at 4°C for 24 h. All subsequent stages were carried out at room temperature. Samples were washed in acetone three times, each time for 20 min, after which they were carefully removed from the microporous pots, and the individual samples were removed from the planchettes. The roots were embedded gradually in TAAB Low-Viscosity Resin (medium) using a graded resin-acetone (v/v) series: 10%, 25%, 50%, 75%, and 100% for 2 h each and 100% resin overnight. Over the next 4 d, the samples were kept in 100% resin with changes twice a day. Individual roots were placed into embedding molds filled with resin and polymerized at 70°C for 24 h.

One-micrometer-thick sections were cut with a Reichert Ultracut E for nanoSIMS analysis. Sections were picked up with a hair and deposited onto a droplet of water on Thermanox coverslips (prepunched to a diameter of 1 cm to fit into the nanoSIMS holders and coated with 20 nm of platinum to make them conducting). Sections were stretched flat on a hotplate. To prevent charging during nanoSIMS analysis, the samples and substrates were coated with a further 10 nm of platinum before loading into the nanoSIMS device.

Analytical Methods

High-resolution SIMS analysis was performed using a CAMECA nanoSIMS 50 device. A focused 16-keV Cs^+ primary ion beam is scanned over the surface of the sample, and the sputtered negative secondary ions are collected and analyzed using a double focusing mass spectrometer. As the bulk concentrations of Si, P, Fe, and As in the samples were relatively low and to avoid potential mass interferences, the detectors for these elements were tuned precisely to the correct position using solid standards of Si, gallium phosphide, a steel sample, and gallium arsenide, respectively. High-resolution mass spectra were acquired from the standards and compared with the signal from the samples to avoid peak overlaps. The region of interest was coarsely selected using the optical camera on the nanoSIMS device and then more accurately using the secondary electron image created by scanning the primary ion beam. To allow quantitative comparisons between the different samples, it was necessary to carefully control the Cs^+ dose applied to the samples. A dose of 1.3×10^{17} Cs^+ ions cm^{-2} was selected from dose-versus-ion intensity curves measured on these samples to just before the maximum signal intensity of the trace elements and allowing time for analysis before the cell walls started to be preferentially sputtered away. Implantation of the Cs^+ (and removal of the platinum and surface contamination) was achieved by continuous scanning of the area of interest with a large, defocused beam for the time calculated to give the required dose determined from the raster area and primary ion current. Ion maps were collected simultaneously for five of the following ions, $^{12}C^{14}N^-$, $^{28}Si^-$, $^{31}P^-$, $^{32}S^-$, $^{56}Fe^{16}O^-$, and $^{75}As^-$, and the secondary electron map. Secondary electrons are produced during the sputtering process, and these can be used to visualize both sample morphology and surface topography. To obtain high-resolution images of the roots, with a size of about 50 μm × 50 μm, the primary aperture was inserted (D1 = 2), which reduced the incident beam size to give a lateral resolution of about 100 nm while still maintaining enough sensitivity to detect the trace elements. Higher resolution images were obtained with smaller apertures reducing the beam size further. Images were acquired with a dwell time of 60 ms at a resolution of 256 × 256 pixels, taking about 1 h per image. NanoSIMS maps are presented in

an arbitrary linear color scale (unless specified), with red and yellow regions indicating higher counts per second and blue and black regions indicating lower counts per second.

Ultrathin sections, approximately 80 nm, were cut using a Reichert Ultracut E Ultramicrotome, stained with uranyl acetate and lead citrate, and observed with a Hitachi 7650 TEM device at 120 keV.

Supplemental Data

The following materials are available in the online version of this article.

Supplemental Figure S1. *lsi2* mutant without Fe plaque.

Supplemental Figure S2. NanoSIMS and TEM image of mature root endodermis.

Supplemental Figure S3. $^{23}NA^{+}$ and $^{40}Ca^{+}$ NanoSIMS images from the stele.

Supplemental Figure S4. TEM image of Fe plaque.

Supplemental Figure S5. Colocalization of S and As in the endodermis of the *lsi2* mutant.

ACKNOWLEDGMENTS

We thank Peter Shewry for advice and for reading through the manuscript.

Received January 27, 2011; accepted April 9, 2011; published April 13, 2011.

LITERATURE CITED

Ali M, Badruzzaman A, Jalil M, Hossain M, Ahmed M, Al Masud A, Kamruzzaman M, Azizur Rahman M (2003) Fate of arsenic extracted with groundwater. *In* M Ahmed, ed, Fate of Arsenic in the Environment. International Training Network, Dhaka, Bangladesh, pp 7–20

Armstrong W (1967) Oxidising activity of roots in waterlogged soils. Physiol Plant **20:** 920–926

Bleeker PM, Hakvoort HWJ, Bliek M, Souer E, Schat H (2006) Enhanced arsenate reduction by a CDC25-like tyrosine phosphatase explains increased phytochelatin accumulation in arsenate-tolerant *Holcus lanatus*. Plant J **45:** 917–929

Bogdan K, Schenk MK (2008) Arsenic in rice (*Oryza sativa* L.) related to dynamics of arsenic and silicic acid in paddy soils. Environ Sci Technol **42:** 7885–7890

Brammer H, Ravenscroft P (2009) Arsenic in groundwater: a threat to sustainable agriculture in South and South-east Asia. Environ Int **35:** 647–654

Burns MS (1982) Applications of secondary ion mass spectrometry (SIMS) in biological research: a review. J Microsc **127:** 237–258

Chandra S, Smith DR, Morrison GH (2000) Subcellular imaging by dynamic SIMS ion microscopy. Anal Chem **72:** 104a–114a

Chen Z, Zhu YG, Liu WJ, Meharg AA (2005) Direct evidence showing the effect of root surface iron plaque on arsenite and arsenate uptake into rice (Oryza sativa) roots. New Phytol **165:** 91–97

Clode PL, Kilburn MR, Jones DL, Stockdale EA, Cliff JB III, Herrmann AM, Murphy DV (2009) In situ mapping of nutrient uptake in the rhizosphere using nanoscale secondary ion mass spectrometry. Plant Physiol **151:** 1751–1757

Cooke R, Kuntz ID (1974) The properties of water in biological systems. Annu Rev Biophys Bioeng **3:** 95–126

Dérue C, Gibouin D, Demarty M, Verdus MC, Lefebvre F, Thellier M, Ripoll C (2006a) Dynamic-SIMS imaging and quantification of inorganic ions in frozen-hydrated plant samples. Microsc Res Tech **69:** 53–63

Dérue C, Gibouin D, Lefebvre F, Studer D, Thellier M, Ripoll C (2006b) Relative sensitivity factors of inorganic cations in frozen-hydrated standards in secondary ion MS analysis. Anal Chem **78:** 2471–2477

Fendorf S, Herbel M, Tufano K, Kocar B (2008) Biogeochemical processes controlling the cycling of arsenic in soils and sediments. *In* A Violante, P Huang, G Gadd, eds, Biophysico-Chemical Processes of Heavy Metals and Metalloids in Soil Environments. Wiley, Chichester, UK, pp 313–338

Follet-Gueye M-L, Verdus M-C, Demarty M, Thellier M, Ripoll C (1998) Cambium pre-activation in beech correlates with a strong temporary increase of calcium in cambium and phloem but not in xylem cells. Cell Calcium **24:** 205–211

Gong HJ, Randall DP, Flowers TJ (2006) Silicon deposition in the root reduces sodium uptake in rice (*Oryza sativa* L.) seedlings by reducing bypass flow. Plant Cell Environ **29:** 1970–1979

Green MS, Etherington JR (1977) Oxidation of ferrous iron by rice (*Oryza sativa* L) roots: mechanism for waterlogging tolerance. J Exp Bot **28:** 678–690

Guerquin-Kern JL, Wu TD, Quintana C, Croisy A (2005) Progress in analytical imaging of the cell by dynamic secondary ion mass spectrometry (SIMS microscopy). Biochim Biophys Acta **1724:** 228–238

Hansel CM, Fendorf S, Sutton S, Newville M (2001) Characterization of Fe plaque and associated metals on the roots of mine-waste impacted aquatic plants. Environ Sci Technol **35:** 3863–3868

Hansel CM, La Force MJ, Fendorf S, Sutton S (2002) Spatial and temporal association of As and Fe species on aquatic plant roots. Environ Sci Technol **36:** 1988–1994

Indriolo E, Na G, Ellis D, Salt DE, Banks JA (2010) A vacuolar arsenite transporter necessary for arsenic tolerance in the arsenic hyperaccumulating fern *Pteris vittata* is missing in flowering plants. Plant Cell **22:** 2045–2057

Kraft ML, Weber PK, Longo ML, Hutcheon ID, Boxer SG (2006) Phase separation of lipid membranes analyzed with high-resolution secondary ion mass spectrometry. Science **313:** 1948–1951

Läuchli A, Kramer D, Pitman MG, Lüttge U (1974) Ultrastructure of xylem parenchyma cells of barley roots in relation to ion transport to the xylem. Planta **119:** 85–99

Li RY, Ago Y, Liu WJ, Mitani N, Feldmann J, McGrath SP, Ma JF, Zhao FJ (2009a) The rice aquaporin Lsi1 mediates uptake of methylated arsenic species. Plant Physiol **150:** 2071–2080

Li RY, Stroud JL, Ma JF, McGrath SP, Zhao FJ (2009b) Mitigation of arsenic accumulation in rice with water management and silicon fertilization. Environ Sci Technol **43:** 3778–3783

Liu WJ, Wood BA, Raab A, McGrath SP, Zhao FJ, Feldmann J (2010) Complexation of arsenite with phytochelatins reduces arsenite efflux and translocation from roots to shoots in Arabidopsis. Plant Physiol **152:** 2211–2221

Liu WJ, Zhu YG, Smith FA, Smith SE (2004) Do iron plaque and genotypes affect arsenate uptake and translocation by rice seedlings (*Oryza sativa* L.) grown in solution culture? J Exp Bot **55:** 1707–1713

Lombi E, Zhao FJ, Fuhrmann M, Ma LQ, McGrath SP (2002) Arsenic distribution and speciation in the fronds of the hyperaccumulator *Pteris vittata*. New Phytol **156:** 195–203

Lux A, Luxova M, Morita S, Abe J, Inanaga S (1999) Endodermal silicification in developing seminal roots of lowland and upland cultivars of rice (*Oryza sativa* L.). Can J Bot **77:** 955–960

Ma JF, Tamai K, Yamaji N, Mitani N, Konishi S, Katsuhara M, Ishiguro M, Murata Y, Yano M (2006) A silicon transporter in rice. Nature **440:** 688–691

Ma JF, Yamaji N (2006) Silicon uptake and accumulation in higher plants. Trends Plant Sci **11:** 392–397

Ma JF, Yamaji N, Mitani N, Tamai K, Konishi S, Fujiwara T, Katsuhara M, Yano M (2007) An efflux transporter of silicon in rice. Nature **448:** 209–212

Ma JF, Yamaji N, Mitani N, Xu X-Y, Su Y-H, McGrath SP, Zhao F-J (2008) Transporters of arsenite in rice and their role in arsenic accumulation in rice grain. Proc Natl Acad Sci USA **105:** 9931–9935

Meharg AA, Rahman MM (2003) Arsenic contamination of Bangladesh paddy field soils: implications for rice contribution to arsenic consumption. Environ Sci Technol **37:** 229–234

Mentré P (1992) Preservation of the diffusible cations for SIMS microscopy. I. A problem related to the state of water in the cell. Biol Cell **74:** 19–30

Metzner R, Schneider HU, Breuer U, Schroeder WH (2008) Imaging nutrient distributions in plant tissue using time-of-flight secondary ion mass spectrometry and scanning electron microscopy. Plant Physiol **147:** 1774–1787

Metzner R, Schneider HU, Breuer U, Thorpe MR, Schurr U, Schroeder WH (2010a) Tracing cationic nutrients from xylem into stem tissue of French bean by stable isotope tracers and cryo-secondary ion mass spectrometry. Plant Physiol **152:** 1030–1043

Metzner R, Thorpe MR, Breuer U, Blümler P, Schurr U, Schneider HU,

Schroeder WH (2010b) Contrasting dynamics of water and mineral nutrients in stems shown by stable isotope tracers and cryo-SIMS. Plant Cell Environ **33:** 1393–1407

Mitani N, Ma JF (2005) Uptake system of silicon in different plant species. J Exp Bot **56:** 1255–1261

Mitani N, Yamaji N, Ma JF (2008) Characterization of substrate specificity of a rice silicon transporter, Lsi1. Pflugers Arch **456:** 679–686

Mondal D, Polya DA (2008) Rice is a major exposure route for arsenic in Chakdaha block, Nadia district, West Bengal, India: a probabilistic risk assessment. Appl Geochem **23:** 2987–2998

Moore KL, Schröder M, Lombi E, Zhao FJ, McGrath SP, Hawkesford MJ, Shewry PR, Grovenor CRM (2010) NanoSIMS analysis of arsenic and selenium in cereal grain. New Phytol **185:** 434–445

Ohno K, Yanase T, Matsuo Y, Kimura T, Rahman MH, Magara Y, Matsui Y (2007) Arsenic intake via water and food by a population living in an arsenic-affected area of Bangladesh. Sci Total Environ **381:** 68–76

Parry DW, Soni SL (1972) Electron-probe microanalysis of silicon in the roots of *Oryza sativa* L. Ann Bot **36:** 781–783

Pickering IJ, Gumaelius L, Harris HH, Prince RC, Hirsch G, Banks JA, Salt DE, George GN (2006) Localizing the biochemical transformations of arsenate in a hyperaccumulating fern. Environ Sci Technol **40:** 5010–5014

Raab A, Schat H, Meharg AA, Feldmann J (2005) Uptake, translocation and transformation of arsenate and arsenite in sunflower (*Helianthus annuus*): formation of arsenic-phytochelatin complexes during exposure to high arsenic concentrations. New Phytol **168:** 551–558

Seyfferth AL, Webb SM, Andrews JC, Fendorf S (2010) Arsenic localization, speciation, and co-occurrence with iron on rice (*Oryza sativa L.*) roots having variable Fe coatings. Environ Sci Technol **44:** 8108–8113

Slodzian G, Daigne B, Girard F, Boust F, Hillion F (1992) Scanning secondary ion analytical microscopy with parallel detection. Biol Cell **74:** 43–50

Smart KE, Smith JAC, Kilburn MR, Martin BGH, Hawes C, Grovenor CRM (2010) High-resolution elemental localization in vacuolate plant cells by nanoscale secondary ion mass spectrometry. Plant J **63:** 870–879

Smith AH, Lingas EO, Rahman M (2000) Contamination of drinking-water by arsenic in Bangladesh: a public health emergency. Bull World Health Organ **78:** 1093–1103

Smith AH, Lopipero PA, Bates MN, Steinmaus CM (2002) Public health: arsenic epidemiology and drinking water standards. Science **296:** 2145–2146

Smith E, Kempson I, Juhasz AL, Weber J, Skinner WM, Gräfe M (2009) Localization and speciation of arsenic and trace elements in rice tissues. Chemosphere **76:** 529–535

Song WY, Park J, Mendoza-Cózatl DG, Suter-Grotemeyer M, Shim D, Hörtensteiner S, Geisler M, Weder B, Rea PA, Rentsch D, et al (2010) Arsenic tolerance in Arabidopsis is mediated by two ABCC-type phytochelatin transporters. Proc Natl Acad Sci USA **107:** 21187–21192

Sparks JP, Chandra S, Derry LA, Parthasarathy MV, Daugherty CS, Griffin R (July 8, 2010) Subcellular localization of silicon and germanium in grass root and leaf tissues by SIMS: evidence for differential and active transport. Biogeochemistry http://dx.doi.org/10.1007/s10533-010-9498-2

Steinbrecht RA, Zierold K (1987) Cryotechniques in Biological Electron Microscopy. Springer-Verlag, Berlin

Su YH, McGrath SP, Zhao FJ (2010) Rice is more efficient in arsenite uptake and translocation than wheat and barley. Plant Soil **328:** 27–34

Vickerman JC, Gilmore IS (2009) Surface Analysis: The Principal Techniques, Ed 2. John Wiley & Sons, Chichester, UK

Wang JR, Zhao FJ, Meharg AA, Raab A, Feldmann J, McGrath SP (2002) Mechanisms of arsenic hyperaccumulation in *Pteris vittata*: uptake kinetics, interactions with phosphate, and arsenic speciation. Plant Physiol **130:** 1552–1561

Williams PN, Islam MR, Adomako EE, Raab A, Hossain SA, Zhu YG, Feldmann J, Meharg AA (2006) Increase in rice grain arsenic for regions of Bangladesh irrigating paddies with elevated arsenic in groundwaters. Environ Sci Technol **40:** 4903–4908

Williams PN, Raab A, Feldmann J, Meharg AA (2007a) Market basket survey shows elevated levels of As in South Central U.S. processed rice compared to California: consequences for human dietary exposure. Environ Sci Technol **41:** 2178–2183

Williams PN, Villada A, Deacon C, Raab A, Figuerola J, Green AJ, Feldmann J, Meharg AA (2007b) Greatly enhanced arsenic shoot assimilation in rice leads to elevated grain levels compared to wheat and barley. Environ Sci Technol **41:** 6854–6859

Wilson RG, Stevie FA, Magee CW (1989) Secondary Ion Mass Spectrometry: A Practical Handbook for Depth Profiling and Bulk Impurity Analysis. Wiley, New York

Xu XY, McGrath SP, Meharg AA, Zhao FJ (2008) Growing rice aerobically markedly decreases arsenic accumulation. Environ Sci Technol **42:** 5574–5579

Xu XY, McGrath SP, Zhao FJ (2007) Rapid reduction of arsenate in the medium mediated by plant roots. New Phytol **176:** 590–599

Yamaji N, Ma JF (2007) Spatial distribution and temporal variation of the rice silicon transporter Lsi1. Plant Physiol **143:** 1306–1313

Zhang W, Cai Y, Tu C, Ma LQ (2002) Arsenic speciation and distribution in an arsenic hyperaccumulating plant. Sci Total Environ **300:** 167–177

Zhao FJ, Ago Y, Mitani N, Li RY, Su YH, Yamaji N, McGrath SP, Ma JF (2010a) The role of the rice aquaporin Lsi1 in arsenite efflux from roots. New Phytol **186:** 392–399

Zhao FJ, Ma JF, Meharg AA, McGrath SP (2009) Arsenic uptake and metabolism in plants. New Phytol **181:** 777–794

Zhao FJ, McGrath SP, Meharg AA (2010b) Arsenic as a food chain contaminant: mechanisms of plant uptake and metabolism and mitigation strategies. Annu Rev Plant Biol **61:** 535–559

Zhao XQ, Mitani N, Yamaji N, Shen RF, Ma JF (2010c) Involvement of silicon influx transporter OsNIP2;1 in selenite uptake in rice. Plant Physiol **153:** 1871–1877